Fractal Patch Antenna based on Photonic Crystal for Enhanced Millimeter-Wave Communication in Intelligent Transportation Systems

Nila Bagheri[1], Jon M. Peha [2], Fernando J. Velez [1]

[1]Instituto de Telecomunicações – DEM Universidade da Beira Interior, Faculdade de Engenharia 6201-001 Covilhã, Portugal, nila.bagheri@ubi.pt, fjv@ubi.pt
[2]Dept. of Electrical and Computer Engineering, Dept. of Engineering & Public Policy, Carnegie Mellon University, Pittsburgh, PA 15213-3890, USA, peha@cmu.edu

Key Points:

- Integrating a microstrip patch antenna on a Photonic Crystals (PhC) substrate improves antenna bandwidth and gain, providing miniaturization.
- By using PhC characteristics, the proposed nonagonal ITS fractal antenna reaches a gain of 10.88 dBi at 38.92 GHz and three resonant bands.
- Photonic Band Gap structures use periodic arranged materials to regulate wave propagation, reducing surface waves, expanding bandwidth.

Corresponding author: Fernando J. Velez, fjv@ubi.pt

Abstract

This paper introduces a Fractal Patch Antenna (FPA) integrated with Photonic Crystals (PhC) designed for Intelligent Transportation Systems (ITS) in the Millimeter-wave bands (mmWaves) given the importance of the application of mmWaves in Vehicle-to-Everything (V2X) networks, we assumed, as examples, that the antenna is designed to resonate at three frequency bands: 31.42 GHz, 37.76 GHz, and 38.92 GHz. With a gain of 10.88 dBi, at 38.92GHz, the antenna demonstrates promising signal reception and transmission capabilities, which are anticipated to be important for ITS operations. The antenna bandwidth covers multiple frequency bands, enabling versatile communication in mmWaves V2X applications. To evaluate the performance of the antenna, we conducted a detailed analysis of its configuration. This included a comparison of the antenna with and without the PhC integration, as well as an exploration of rectangular lattice structure. In addition, variations in hole sizes and spacing were examined to assess their impact on key parameters such as the gain and reflection coefficient. The integration of fractal geometry and PhC structures results in a compact, high-performance antenna suitable for mmWave communication. The integration of fractal geometry and PhC structure results in compactness and high performance in mmWaves communication applications. Through simulation and analysis, including radiation pattern, gain, and reflection coefficient plot assessment, the antenna performance is thoroughly evaluated. The study highlights the potential of the proposed FPA-PhC antenna configuration to enhance communication networks within the ITS, significantly advancing the ITS system with support from the mmWave bands.

Plain Language Summary

This study introduces a Fractal Patch Antenna (FPA) integrated with Photonic Crystals (PhC) to improve communication within Intelligent Transportation Systems (ITS) by leveraging millimeter-wave (mmWave) bands. The antenna is designed to operate efficiently at frequencies of 31.42 GHz, 37.76 GHz, and 38.92 GHz, achieving a high gain of 10.88 dBi at 38.92 GHz, which improves its ability to send and receive signals. With a broad bandwidth covering multiple frequencies, it supports versatile applications, particularly in Vehicle-to-Everything communication. We have conducted a comparative analysis between the FPA with and without the PhC, as well as variations in rectangular lattice configurations and changes in hole sizes and spacing. The use of fractal geometry and PhC with square lattice ensures compactness while significantly improving performance. Comprehensive simulations and analyses of key parameters such as radiation patterns, gain, and reflection coefficients validate the antenna's capability, demonstrating its potential to advance ITS communication networks and enable efficient mmWave communications.

1 INTRODUCTION

Every year, millions of road accidents could be prevented with advanced vehicle communication systems. Vehicle-to-Everything (V2X) technology, particularly using millimeter-wave (mmWave) bands, promises to transform road safety with higher data rates. This highlights the importance of developing antennas that operate efficiently at high frequencies, enabling high-speed communication between vehicles and the infrastructure. mmWave frequencies are

particularly suited for short-range, high-data-rate applications in dense urban environments where infrastructure can support the deployment of small cells and repeaters. These antennas are essential for leveraging the high data rates and low latency offered by the mmWave bands, facilitating advanced V2X communication systems. A Fractal Patch Antenna (FPA) based on Photonic Crystals (PhC) is a type of antenna that utilizes fractal geometry and PhC to achieve enhanced performance compared to traditional patch antennas. Howell (Howell, 1975) first introduced the microstrip antenna in 1972, with the patch antenna representing a variant of the compact antenna design. Patch antennas can take various forms, including circular, rectangular, triangular, and square shapes, with different feeding methods available. While patch antennas offer advantages such as lightweight construction, minimal manufacturing costs, operation at microwave frequencies, compatibility with integrated circuit technology, and compactness, they suffer from poor gain. This paper is organized to systematically explore and compare antenna configurations for improved V2X communication. Not only does one delve into the design and analysis of antennas with square lattice photonic crystals, but one also discusses the antenna design without PhC integration. Antennas with square lattice photonic crystals are then compared with rectangular lattice designs, highlighting differences in gain and bandwidth performance. The effects of varying the size and spacing of PhC on the antenna's performance are explored as well, providing insights into the tunability and adaptability of these configurations in practical deployments.

1.1 Background

Various scenarios have been proposed to achieve the required high gain and high bandwidth by including the utilization of metamaterials as substrates (Soily et al., 2022; Hamza et al., 2022; K & Pradeep, 2022; Sinha et al., 2021; Deshmukh et al., 2019, 2019), parasitic patches (Awan et al., 2021; Sharma et al., 2021; El Arrouch et al., 2022; Erbaş, 2020; Oliveira et al., 2021; Hossain et al., 2021; Asok & Dey, 2021), air gaps (Tanveer et al., 2021), slots (J. Zhang & Mao, 2020; Khabba et al., 2022; Mangal & Gour, 2021; Lin & Omote, 2021; Olawoye & Kumar, 2020; Hao et al., 2020; C. Chen, 2022), shorting pins (Yang et al., 2021; Fang et al., 2022; Gautam & Kumar, 2023; Wu et al., 2023; Ahmad et al., 2020, 2020; X. Zhang et al., 2021), metamaterials (Sufian et al., 2021; Kulkarni & Deshpande, 2024; Mishra et al., 2023; Bakir & Sahin, 2023; Yin et al., 2023; Kumar et al., 2023), dielectric substrates (Dong et al., 2022; Desai & Bindu, 2023; Jiang et al., 2023; Li et al., 2023; Muangrung et al., 2023), antenna array (Yan et al., 2024), configurations, multilayered substrate techniques (Zhao et al., 2023), and incomplete grounds (Biswas et al., 2023). Furthermore, the use of PhC structures has been proposed to address surface waves (Messatfa et al., 2022; Benlakehal et al., 2024, 2023, 2022; Saurabh & Meshram, 2022; Temmar et al., 2023). PhC, periodic dielectric structures, prohibit electromagnetic waves of specific directions from passing through them (Messatfa et al., 2022; Salehi et al., 2020). Beyond 5G and 6G networks promise transformative capabilities, including high data rates, low latency, and massive connectivity, making them well-suited for enhancing Intelligent Transportation Systems (ITS) functionalities. The design of the antenna presented uses the concept of fractal geometry, which involves repeating patterns at different scales. Incorporating fractal elements into the patch structure enables us to achieve a more compact antenna size without destroying performance. Miniaturization is crucial for the integration of the antenna into small, space-constrained devices commonly found in ITS. A key aspect of antenna design is the use

of a PhC as a substrate material. PhC are materials that show unique electromagnetic properties, including control over the propagation of waves.

1.2 The True Reasons for Designing V2X Antennas in the Millimeter Wave Bands

Advances in wireless communications, particularly intelligent vehicular communications, require frequency spectrum allocation and management strategies that accommodate the increasing demand for bandwidth, efficiently utilize it, and mitigate interference.

The functionality of Autonomous and Connected Vehicles (ACVs) relies on data from various sensors, necessitating high communication bandwidths, often in the gigabits-per-second range. mmWave technology is crucial for achieving this, enabling high-performance Vehicle-to-Vehicle (V2V), Vehicle-to-Infrastructure (V2I), and intra-vehicular communications. mmWave V2V links allow vehicles to share raw data with neighboring vehicles, enhancing situational awareness. V2I links use mmWave to improve road safety applications by transmitting vehicle data to cloud resources for processing. mmWave links with high data rate are also used to download real-time maps and dynamic environment information (Hakak et al., 2023). ACVs utilize various mmWave communication bands, including 5G bands like 28 GHz, unlicensed bands like 60 GHz, and automotive radar bands like 24 GHz and 76 GHz (Ahangar et al., 2021). However, designing 5G antennas for autonomous vehicles poses significant challenges (Saad et al., 2023), as these antennas must provide reliable communication with a wide radiation pattern and a wide operating frequency range.

The author in (Mukherjee, Roy, & Mukhopadhyay, 2022) presents a SISO antenna in Y shape designed to cover the (26.5 - 28) GHz, 5G mmWave bands. This paper also provides a comparison between the proposed SISO antenna and current MIMO antennas used in automotive applications. Traditionally, licensed sub-6 GHz bands such as 2.4 GHz and 5.9 GHz have been commonly used for ITS (Soto et al., 2022). However, the emerging 26.5 GHz and 28 GHz mmWave 5G bands (Mukherjee, Mukhopadhyay, & Roy, 2022) are being explored for ITS due to their potential to enable much faster data rates and lower latency compared to sub-6 GHz bands (Mukherjee et al., 2020). This capability is crucial for V2V communication, which is essential for automated driving, optimizing fuel efficiency, and providing rapid communication to prevent breakdowns. In (Niranjan Prasad et al., 2023), the design and analysis of a wideband 5G antenna for autonomous vehicles is discussed. The proposed antenna utilizes Tesla geometry, which is known for its high gain and wide-angle radiation pattern. The results show a gain of 4.5 dB, a bandwidth of 2.442 GHz, and an operational frequency of 29.2 GHz. In (Saad et al., 2023), the design of NR V2X SL communication prioritizes the FR2 (24.25 – 52) GHz band to support high data rates (50-1000) Mb/s. Beamforming is essential to counteract pathloss at higher frequencies and can also be used for FR1. It enables directional transmission, facilitates spatial reuse of resources in congested areas, and expands the coverage of the V2X network. Additionally, beamforming allows controlled sidelink power.

The mmWaves offer the potential for achieving ultra-high data rates, which are essential for supporting these advanced applications. With limited available spectrum below 6 GHz, it is challenging to meet the required data rates for advanced V2X applications. The mmWaves provide a large transmission bandwidth, which can help address the scarcity of spectrum and sup-

port the high data rate demand of V2X communications. Despite the challenges posed by high atmospheric attenuation and significant path loss in the mmWaves channel, specific beamforming can mitigate these issues by concentrating the transmitted signal in one direction (D. Zhang et al., 2018).

As a fundamental aspect of ITS, the utilization of beyond 5G (B5G) technology in V2X communication has garnered global attention. This cutting-edge technology promises to revolutionize the way vehicles interact with each other (V2V) and with infrastructure (V2I), improving safety on roads (Ye et al., 2024).

The 3rd Generation Partnership Project (3GPP) has acknowledged the performance challenges inherent in V2X communication and addressed them in its Release 17. This release standard stipulates that the 5G new radio (NR) frequency range 2 (FR2), spanning from 24 GHz to 71 GHz, can be employed for V2X communication. However, several challenges arise when operating in this high-frequency band.

The advent of 5G NR technology has brought about significant advancements in vehicular communication, particularly in the context of V2X networks (Gyawali et al., 2021). V2X networks encompass various types of communication between vehicles, infrastructure, pedestrians, and other entities, enabling better road safety and enhanced driving experiences (Garcia et al., 2021). One key aspect of 5G NR-based V2X communication is its use of high communication frequencies in the FR2 spectrum, which offers increased spectrum resources in V2I communication scenarios (Saad et al., 2021). In the 3GPP Release 17 standard, the upper bound of the FR2 spectrum has been extended to 71GHz. As a result, high-frequency wireless communication can be expected to play a significant role in future B5G V2X networks (3GPP, 2021; 3rd Generation Partnership Project (3GPP), 2023). In summary, while there are challenges to overcome, mmWaves with ongoing research and development efforts focused on enabling technologies, mmWaves NR-V2X could indeed be a suitable option to enhance V2X communication capabilities (S. Chen et al., 2024; Saad et al., 2023). Sidelink communications, in the context of wireless networking, refer to a mode of direct communication between devices without the need for intermediation by a central network infrastructure. It allows devices to establish peer-to-peer connections, enabling efficient data exchange and collaboration, particularly in scenarios where direct communication is beneficial, such as V2V communication in ITS or device-to-device (D2D) communication in crowded urban environments. Some argue that there is not enough spectrum in the Intelligent Transportation System (ITS) band to meet the needs of V2X communications. One way to address this problem is to make the spectrum available somewhere in the FR2 bands. That is the approach taken in this paper. Another way to address that problem is to give V2X devices access to bands that are currently unlicensed as proposed in (Peha, 2023; Peha et al., 2024), because sharing between V2X devices and unlicensed devices can be very efficient (Ligo & Peha, 2019). The 3GPP Release 17 & 18 for the next generation of V2X will support operations in the FR2 spectrum range, which is from 24.25 GHz to 71 GHz (Saad et al., 2023), and researchers have been exploring the use of mmwave spectrum for V2X. It is not yet known which spectrum band at these higher frequencies will be used. The October 2024 V2X interoperability demonstration in Cheyenne, Wyoming, revealed that some participants were exploring the use of complementary spectrum beyond the 5.9 GHz band, reflecting a growing interest in leveraging alternative frequency ranges for advanced V2X applications (U.S. Department of Trans-

portation (October), 2024). For this research, as an example, we designed an antenna that operates at 31.42 GHz, 37.76 GHz, and 38.92 GHz.

1.3 Proposed Approach

The proposed FPA offers significant advantages in facilitating V2I communication. The use of fractal geometry combined with the PhC structure allows the antenna to operate on a wide range of frequencies, providing increased bandwidth for data transmission. This allows for the transmission of big data at high data rates, essential for supporting applications such as real-time video feeds and V2V communications. FPAs are known for their compact and low-profile design, making them ideal for integration into vehicles without adding significant bulk or altering the vehicle's aerodynamics.

The proposed FPA offers significant advantages for V2I communication. The combination of fractal geometry and PhC structure enables the antenna to operate over a wide range of frequencies, increasing bandwidth for data transmission. This capability supports high- data-rate applications such as real-time video feeds and V2V communications. Known for their compact and low-profile design, FPAs are ideal for vehicle integration without adding significant bulk or altering aerodynamics. This versatility allows for seamless integration with existing communication infrastructures and supports future advancements in vehicular communication. By integrating the antenna into vehicles, they can establish reliable and high data-rate links with roadside infrastructure such as traffic lights, road signs, and traffic management systems.

Additionally, the antenna facilitates communication with toll systems, parking meters, and charging stations, allowing seamless and efficient services such as automated toll payments and electric vehicle charging coordination. In the realm of Vehicle-to-Pedestrian (V2P) communications, the FPA plays a crucial role in improving road safety. By equipping vehicles with antenna, they can establish short-range wireless connections with pedestrian devices, such as smartphones or wearable devices. FPA enables real-time exchange of information, warnings, and alerts, allowing vehicles to inform pedestrians of their presence when approaching crosswalks or provide warnings in the event of potential collisions. This type of communication fosters safer interactions between vehicles and pedestrians, contributing to overall road safety.

Moreover, the FPA facilitates seamless V2V communication, essential to improve traffic safety and efficiency. Integrating the antenna into vehicles enables them to establish direct wireless links with nearby vehicles, facilitating the real-time exchange of information such as vehicle position, speed, and trajectory. This enables collaborative collision avoidance and cooperative adaptive cruise control, among other applications, leading to safer and more efficient traffic flow.

To evaluate the performance of the FPA, extensive simulations are performed using the high-frequency structural simulation instrument HFSS, (Ansys, 2023). The analysis encompassed parameters such as radiation patterns, gain, and bandwidth. The results obtained from these simulations examine the exceptional gain characteristics of the proposed antenna in the millimeter-wave ITS range, which align well with the anticipated requirements for ITS. Relevantly, the importance of the application of mmWaves in V2X networks led us to assume, as examples, that the antenna resonates at three key frequencies: 31.42 GHz, 37.76 GHz and 38.92 GHz, aligning with the future frequency spectrum for ITS applications.

1.4 Structure of the Paper

To rest of the paper, organized as follows: Section 2 explores the integration of PhC antennas for augmented performance, with a specific focus on the future potentials and implications of PhC antennas in V2X communications. Section 3 examines the critical aspects of antenna design and performance analysis and includes the analysis of the reflection coefficient (S11) plot for three resonance bands, radiation pattern plot, gain plot and directivity plot along with the 3D radiation pattern. The study includes a detailed comparison of different lattice geometries, such as, square lattices, antenna without PhC, and rectangular lattices whilst evaluating the impact of the hole and space size variations on parameters such as S11 and gain. In Section 4 the antenna is introduced, highlighting its compact design, beyond 5G capabilities, and potential contributions to the advancement of communication technologies and V2V. Finally, Section 5 presents the conclusions and summarizes the findings of the study, offering an overview of the primary contributions and briefly outlining suggestions for future research.

2 ANTENNA DESIGN

Antenna design involves engineering the antenna structure and its associated components to enhance its performance for a given application. The appropriate type of antenna (such as a dipole or patch antenna), the size and shape of the antenna, and the materials used to fabricate it are essential considerations. To ensure that the antenna meets the desired specifications in terms of gain, directivity, and radiation pattern, the design process includes simulation and testing. In the study, a copper nonagon is chosen as a radiation patch.

Fig. 1(a) shows the microstrip antenna configuration proposed for the triple band antenna. The antenna design is implemented on a Gallium Arsenide (GaAr) substrate with dimensions $L_s \times W_s \times h = 4.9 \times 5.9 \times 1\,\text{mm}^3$, $r_o = 0.85\,\text{mm}$, $r_i = 0.5\,\text{mm}$, and $L_m = 0.7\,\text{mm}$ and ε_r=12.9.

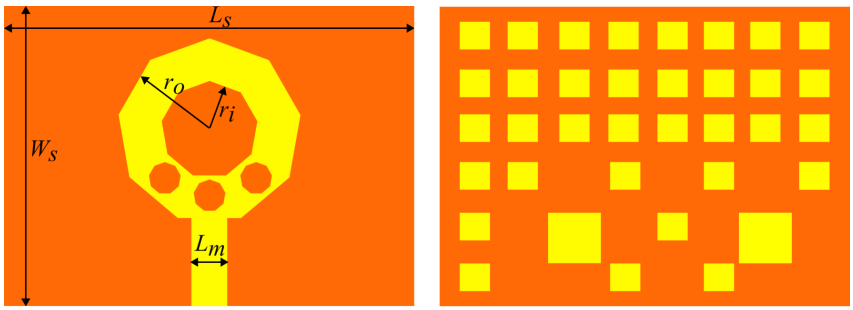

Figure 1. (a) Configuration of the proposed microstrip patch antenna, illustrating its dimensions and layout fig.a.
(b) Structure of the square lattice photonic crystal used for the ground and substrate of the antenna fig.b.

The shape of the antenna is a regular nonagon made of copper, with three nonagonal fractals created in it, the thickness of the copper patch is 0.035 mm, it is fed by a 50 Ω microstrip line, with a strip width of 0.9 mm. The height

of the ground copper is 0.035 mm. PhC substrate is created by integrating the cuboid in a bed with a diagonal of 0.2 mm and a distance between each cuboid of 1 mm. As mentioned earlier, reducing the size of the cuboids and increasing the distance between the cylinders will reduce the gain and bandwidth of the antenna.

Fig. 1 (b), shows the structure of PhC for the ground and substrate. The structure of a PhC consists of a periodic arrangement of dielectric materials with alternating high and low refractive indices. Periodicity creates a photonic bandgap, a range of frequencies where light propagation is forbidden, similar to the bandgap in semiconductors for electrons. These bandgaps are crucial for controlling the flow of light, enabling applications such as waveguiding, filtering, and optical sensing. Hence, the introduction of defects within the PhC lattice is a key strategy for modifying the optical properties. These defect modes act as resonators, prohibiting or guiding light at specific frequencies, thus enabling functionalities such as efficient light emission, high-Q optical cavities, and enhanced sensing capabilities.

2.1 Mathematical Equations

To design a patch antenna, it is important to consider several equations. The equations considered to calculate the patch length are as follows:

$$L = \frac{c}{2f_0\sqrt{\varepsilon_{eff}}} - 0.824h\left(\frac{(\varepsilon_{eff}+0.3)\left(\frac{W}{h}+0.264\right)}{(\varepsilon_{eff}-0.258)\left(\frac{W}{h}+0.8\right)}\right) \tag{1}$$

where L is length of the patch, c is the speed of light, W is width of the patch, ε_{eff}, is the effective dielectric constant, f_0 is the operating frequency of the antenna and h is the height/thickness of the substrate. The patch width, W, can be calculated as follows:

$$W = \frac{c}{2f_0\sqrt{\frac{\varepsilon_R+1}{2}}} \tag{2}$$

where ε_R is the value of the dielectric constant of the substrate. The effective dielectric constant is calculated as follows:

$$\varepsilon_{eff} = \frac{\varepsilon_R+1}{2} + \frac{\varepsilon_R-1}{2}\left[\frac{1}{1+12\left(\frac{W}{h}\right)}\right] \tag{3}$$

For the patch antenna, impedance matching techniques are considered to ensure maximum power transfer to the antenna and that the element can strongly radiate and contains matching of the input impedance at the end of the antenna's feedline (to the feedline's characteristic impedance).

2.2 Photonic Band Gap Structure

A PhC is a periodic structure that exhibits a spatial variation in its dielectric properties, causing it to interact with light in unique ways. Much like how the arrangement of atoms in a crystal lattice affects the behavior of electrons in a material, the periodic arrangement of dielectric materials on PhC affects the propagation of electromagnetic waves (light) within it. PhC can be designed by creating holes or rod shapes in the structure of the antenna substrate. By changing the radius and size of the holes or rods shape and changing the distance between those, the gain, bandwidth and other features of the antenna changes.

In two-dimensional PhC design, there are several types of lattices. (hexagonal, square, and rectangular) are considered along with five different shapes of scatterers: hexagonal, circle, square, rectangle, and oval. These scatterers are considered as dielectric rods in air, or air rods are modeled in dielectric media. This choice of configurations underscores the significant effect of lattice symmetry and scatterer geometry on the size of the PBG. The schematic of a photonic crystal lattice in a PhC presented in Fig. 2 offers precise control over the propagation of light.

A Bravais lattice describes the periodic arrangement of points in space, forming the foundation of crystal structures, including applications in photonic crystals. In two dimensions, common types of structures include square, hexagonal, and rectangular lattices. These structures define how electromagnetic waves interact with the material and directly influence the propagation of the waves. In square lattices, antenna elements are arranged symmetrically and periodically, leading to a uniform and predictable radiation pattern. The square lattice simplifies the design and implementation of antenna arrays, ultimately justifying this adoption for systems that require simple and stable radiation patterns. In phased array antennas, square lattices allow precise beam steering and help reduce side lobes. In a square lattice, the elements are equally spaced along the x and y axes, ensuring a uniform distance in all directions. The high symmetry produces a consistent radiation pattern as elements harmoniously contribute to the final outcome with similar phases. This arrangement prevents signal fluctuations and irregularities in different directions. While a hexagonal lattice has equal side lengths ($a = b$) with angles between adjacent vectors of 120°, a rectangular lattice has unequal side lengths ($a \neq b$) with angles between adjacent vectors of 90°. On the other hand, a square lattice has equal side lengths ($a = b$) with angles between adjacent vectors of 90°, and is often preferred in antenna application, mainly due to its simplicity, uniform spacing, and symmetrical properties.

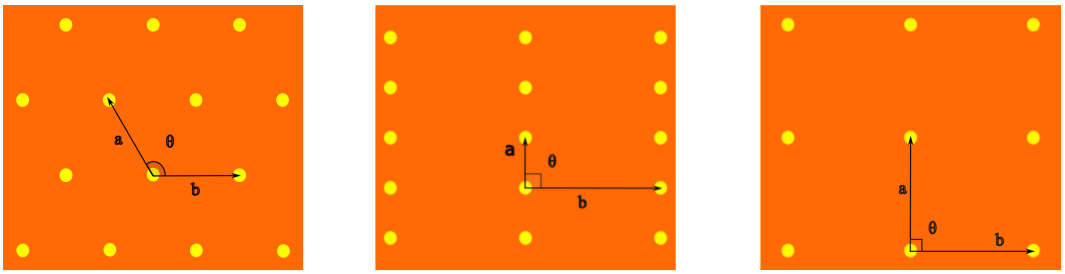

(a) (b) (c)

Figure 2. The three fundamental two-dimensional Bravais lattices: (a) Hexagonal lattice: $|a| = |b|, \theta = 120°$; (b) Rectangular lattice: $|a| \neq |b|, \theta = 90°$; (c) Square lattice: $|a| = |b|, \theta = 90°$.

Defects in this lattice structure enhance functionality, tunability, sensing capabilities, and fault tolerance. They enable tailored optical or frequency responses, tunable properties, sensing of environmental changes. Inclusion of defects expands the application in photonics and optical communication systems. A square-shaped PhC has been utilized for the design of the proposed antenna. These shapes can provide additional degrees of freedom in tuning the PBG compared to other structures. For example, square lattices can exhibit different symmetry properties and may support different types of photonic band gap compared to other lattices. Fig. 2 schematic representations

of different PhC lattice configurations provide insight into their structural diversity.

Photonic Band Gap (PBG) materials are periodic and display broadband pass and stop band attributes at microwave frequencies. PBG components are composed by introducing periodic disturbances such as PhC rods, cavities, and patterns in waveguides and substrates. As in PhC photon propagation, the electromagnetic waves in a PBG structure are impeded because of the periodic discontinuity, hence making a slow wave structure. Within the PBG, the modes of EM wave propagation have field distributions and dispersion properties that differ significantly from those in free space. Due to these unique properties of PBG materials, they have potential applications in antennas, amplifiers, waveguides, and filters, power combining, phased arrays, EMC measurements, and many microwave devices. Employing this method improves gain, suppresses surface waves, and increases antenna bandwidth, while reducing patch loss.

In a recent study of ours (Bagheri et al., 2024), the performance of a similar photonic crystal antenna was analyzed with and without the integration of the PhC structure. In that study, the results have clearly demonstrated the significant enhancements in gain and bandwidth achieved by incorporating the PhC substrate compared to that achieved by incorporating the conventional configuration. This comparative analysis underscores the effectiveness of the PhC structure in improving the overall performance of this type of antennas. Besides, the authors of (Vahdati & Parandin, 2019), have proposed the establishment of a photonic crystal surface that enables antennas to achieve uniform electromagnetic radiation. Adjusting the underlying microstrip layer beneath the crystalline layer has shown to expand the bandwidth in the 30-80 GHz range by as much as approximately 50 GHz. Furthermore, the antenna gain has improved from 6.45 dB to 7.7 dB, reflecting an increase of about 1.2 dB. These improvements clearly show that incorporating the crystal layer leads to a significant enhancement of the bandwidth and gain of the antennas, particularly when operating at terahertz frequencies.

GaAs was selected as the primary material for the proposed antenna substrate due to its customized properties. GaAs acts as a semiconductor with distinct advantages: it offers superior electron mobility crucial for effective operation at high frequencies, a wide bandgap essential for achieving high-speed data transmission, and a lower noise figure resulting in improved signal clarity.

Furthermore, GaAs demonstrates a higher breakdown voltage, enhancing antenna durability, maintains consistent electrical properties across a broad range of temperatures, providing reliable performance, and features a low-loss tangent, minimizing energy loss. GaAs possesses relatively high thermal conductivity, facilitating efficient heat dissipation, thus maintaining antenna performance over extended periods.

In the proposed design, we introduce square holes in the GaAs substrate, beneath the FPA, to create a PhC structure. This modification offers several benefits. The periodic arrangement of square holes forms a PBG, this allows precise control over transmission and reflection, enhancing antenna performance. The PhC structure influences radiation patterns, enabling directional beams or beam steering. Modifying the size and arrangement of holes customizes the radiation properties for specific applications. The structure confines electromagnetic energy within the antenna, minimizing substrate losses and enhancing radiation efficiency. Adjusting hole size and spacing tunes PBG

and dispersion characteristics, improving antenna performance for the desired parameters.

The defect design offers precise control over the band gap properties of PhC substrates, enhancing the antenna's performance and versatility. By strategically designing defects, the band-gap characteristics can be tailored to specific frequency ranges, improving frequency selectivity and spectral efficiency. These defects induce localized resonant modes within the band gap, which can be finely tuned to adjust the antenna's operating frequency or bandwidth.

According to (Roslan et al., 2018), the performance of photonic crystal cavity (PCC) antennas, including resonant frequency, S parameters, gain, and radiation pattern, is highly sensitive to variations in hole size and spacing. A radius of 9.6 µm resulted in a return loss of -71.94 dB and a gain of 9.730 dB, while a spacing of 100.1 µm achieved a return loss of -56.56 dB and a gain of 9.726 dB. These findings demonstrate that precise geometric adjustments are essential for effective photonic bandgap control.

Strategically placed defects manipulate the radiation properties of the antenna whilst introducing phase shifts and altering propagation directions. Enhancing the antenna's beam steering capabilities allows it to dynamically adjust its radiation pattern and track moving targets. Defects also mitigate losses within the substrate, enhancing radiation efficiency by minimizing scattering and re-absorption of electromagnetic waves. Improvement in energy transfer from the antenna to the surrounding environment improves overall performance.

3 Results and Discussion

The diagram of the reflection coefficient (S11) of the PhC square lattice is shown in Fig. 3. This antenna exhibits three resonance bands at 31.42, 37.76 and 38.92 GHz covering frequency bandwidths of 1.73 GHz, 0.38 GHz and 0.78 GHz, in the ranges of [30.82, 32.55 GHz], [37.53, 37.91 GHz], and [38.40, 39.18 GHz] with a total bandwidth of 2.89 GHz. These bands are part of the K_a-band in mmWaves. The resonance bands at 31.42 GHz, 37.76 GHz and 38.92 GHz exhibit sharp dips with reflection coefficients of -17.48 dB, -24.47 dB and -41.02 dB, respectively. The antenna with square lattice includes square-shaped holes, where each side is 0.2 mm in length and the gap between adjacent holes is 0.4 mm, which contributed to its superior performance by enhancing constructive interference.

The S11 diagram illustrates how much electromagnetic energy is reflected back from the antenna across different frequencies. It consists of a plot showing the magnitude (in dB) of the reflection coefficient versus the frequency. Peaks or dips in the plot indicate the frequencies in resonance that the antenna is most efficient. The wider bandwidth indicates the broader frequency coverage. The diagram helps improve antenna design for efficient communication.

The fine-tuning of the proposed antenna was achieved through improving its impedance matching, demonstrating satisfactory performance across three frequency bands (31.42 GHz, 37.76 GHz), and 38.92 GHz, and providing appropriate impedance matching in these ranges. As shown in Fig. 4, the values of VSWR and S11 confirm efficient power transfer and reduced signal reflection, ensuring enhanced performance.

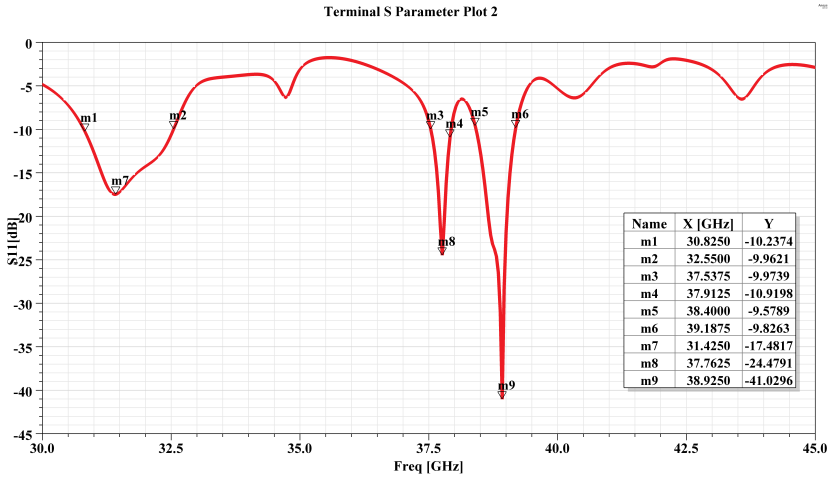

Figure 3. Reflection coefficient plot for the proposed PhC antenna with square lattice.

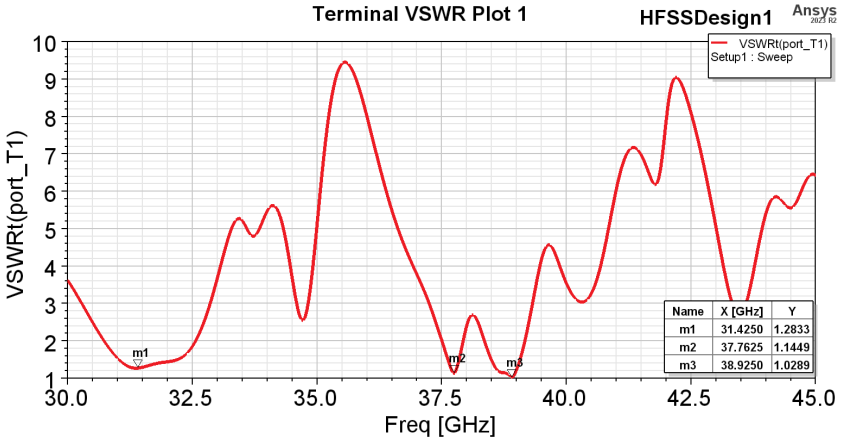

Figure 4. Plot of the VSWR for the proposed PhC antenna with square lattice.

In antenna design, a VSWR below 1.5 is considered excellent, while values up to 2.0 are generally acceptable for most communication applications. Similarly, a S11 value lower than -10 dB is typically regarded as acceptable, whereas values of -15 dB, or lower, indicate very good performance.

At 31.42 GHz, the VSWR is 1.28, and the S11 is -17.48 dB, indicating appropriate impedance matching in the antenna with the square lattice. At 37.76 GHz, the VSWR is 1.14, and S11 is -24.47 dB, reflecting improved performance in this band. At 38.92 GHz, the VSWR reaches 1.02, with an S11 of -41.02 dB, showing minimal reflection and maximum efficiency in this frequency range. The obtained results confirm that the proposed antenna exhibits stable operation across the intended frequency bands and meets the industry-standard impedance matching requirements. The low VSWR and deep S11 values indicate excellent signal transmission with minimal return losses, making this design highly suitable for millimeter-wave communication applications within ITS.

In Fig. 5 the radiation pattern plot illustrates how electromagnetic energy is distributed in different directions from the antenna in three frequency

bands 31.42 GHz, 37.76 GHz and 38.92 GHz. It shows the intensity of radiation in angular coordinates relative to the antenna's orientation. The main lobe represents the direction of maximum radiation, whereas the side lobes indicate the directions of secondary radiation. The plot helps to determine the antenna's coverage area, directivity, and suitability for specific applications. The radiation pattern plot illustrates the distribution of electromagnetic energy in various directions from the antenna, across three resonant frequency bands.

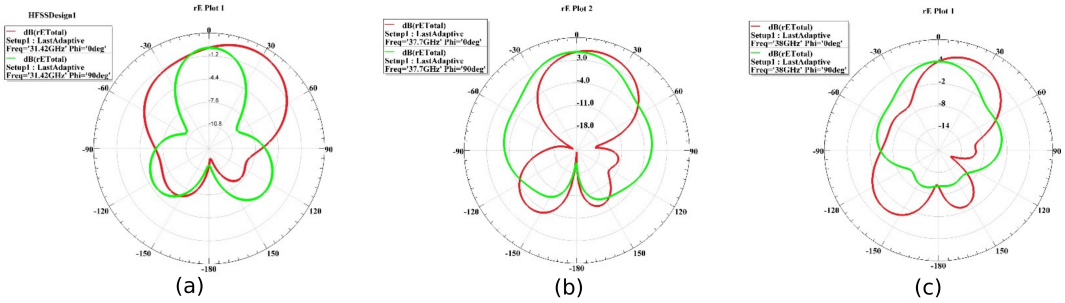

Figure 5. Radiation pattern plot for the proposed PhC antenna with square lattice, at (a) 31.42 GHz, (b) 37.76 GHz, (c) 38.92 GHz.

In Fig. 6, the gain plot shows the antenna gain characteristics in the 31.42 GHz, 37.76 GHz, 38.92 GHz frequencies. It shows the gain and directivity compared to that of an ideal isotropic radiator. The gain plot provides information on the antenna's ability to focus radiation in desired directions, aiding in the assessment of its directional performance and efficiency. Fig. 7 which shows the directivity plots for the proposed antenna at the three resonant frequencies. These plots demonstrate the antenna's ability to effectively concentrate radiation in specific directions, achieving commendable directivity values of 4.34 dB at 31.42 GHz, 8.28 dB at 37.76 GHz, and 8.86 dB at 38.92 GHz. Fig. 8 illustrates the antenna gain plot without the PhC. At 31.42 GHz, the gain was 5.52 dB, indicating weaker impedance matching. At 37.76 GHz and 38.92 GHz, the gains were 4.58 dB and 6.15 dB, respectively, with broader radiation patterns. In contrast, the achieved gain plot with the PhC square lattice shown in Fig. 6, highlights a significant increase in gain resulting from the incorporation of PhC. Inclusion of PhC not only enhances the gain of the antenna, but also improves its directivity by enabling more focused radiation patterns. This optimized design utilizes the PhC's properties to effectively concentrate energy in specific directions, leading to improved signal radiation performance and clearly demonstrate the critical role of PhC in advanced antenna design, for applications that require high gain and precise directivity. As shown in Fig. 9 by analyzing the S11 plot of the antenna without the PhC structure, it is possible to observe a considerable decrease in bandwidth, compared to the performance of the antenna that uses PhC. The antenna bandwidth increases from 1.50 GHz without the photonic crystal to 2.89 GHz with the incorporation of the photonic crystal. Fig. 10 shows the reflection coefficient plot for the antenna with rectangular lattice structure. The resulting bandwidth for this design is only 1.41 GHz, indicating moderate impedance matching and a relatively narrower operational range. The increased bandwidth in the antenna with the square lattice structure highlights its superior performance. Showing that it is more suitable for applications that demand both precise impedance matching and wider frequency coverage, these find-

ings emphasize the role of lattice geometric in optimizing antenna bandwidth and overall efficiency for specific applications.

At 31.42 GHz, the gains for PhC antennas with the square lattice and rectangular lattice structures are nearly identical. The square lattice PhC antenna (whose gain plots are shown in Fig. 6 (a)) demonstrates better directionality characteristics, while the rectangular lattice one exhibits a broader radiation pattern, as shown in Fig. 11 (a). At 37.76 GHz, the gain of the square lattice antenna from Fig. 6 (b) significantly outperforms the gain of the rectangular lattice antenna in Fig. 11 (b). It achieves a gain of 8.48 dB compared to 4.69 dB (for the rectangular one), with a more focused and directional radiation pattern. Similarly, at 38.92 GHz, the gain of the square lattice antenna presented in Fig. 6 (c) is higher (8.73 dB) and demonstrates superior directionality compared to the rectangular lattice antenna, whose gain is 7.06 dB (Fig. 11) (c). These results highlight the advantages of square lattice structures in terms of gain and radiation pattern.

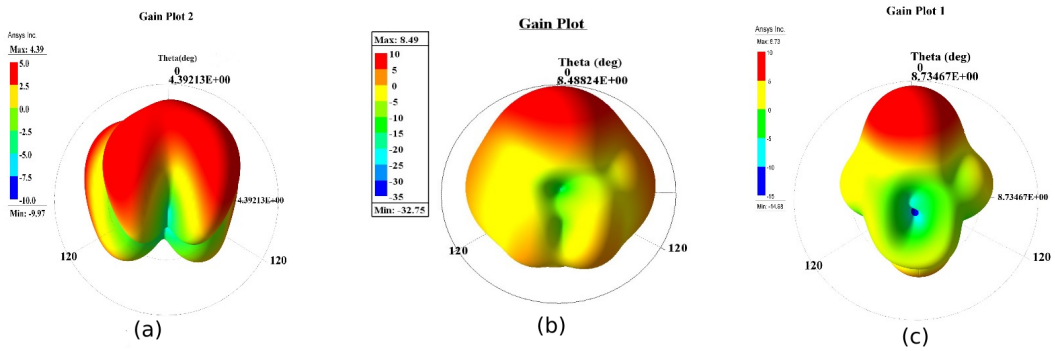

Figure 6. Gain plot for the proposed PhC microstrip patch antenna with square lattice, at (a) 31.42 GHz, (b) 37.76 GHz, (c) 38.92 GHz.

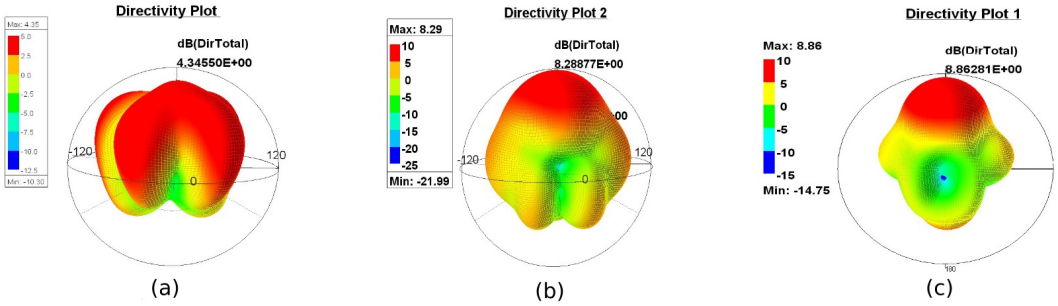

Figure 7. Directivity plot for the proposed PhC antenna with square lattice, at (a) 31.42 GHz, (b) 37.76 GHz, (c) 38.92 GHz.

Table 1 presents a brief comparison of antenna performance metrics across different materials and frequency bands.

It provides insights into key parameters such as gain, bandwidth, and frequency for materials such as FR-4, TLY-5, and GaAs. The tabulated data facilitate rapid assessment of each material's suitability for specific frequency

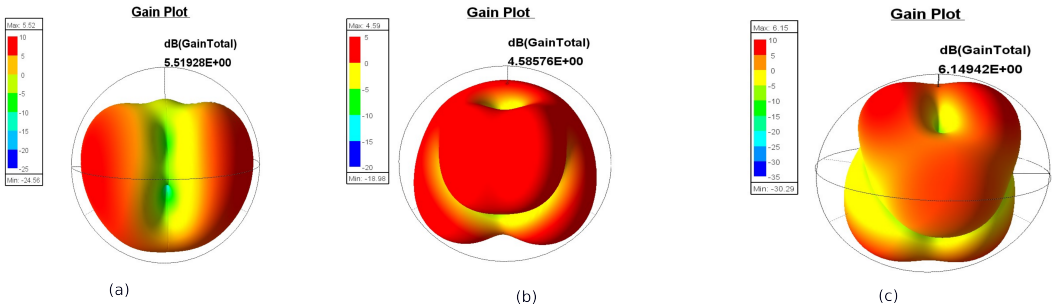

Figure 8. Gain of the antenna without PhC structure at (a) 31.42 GHz, (b) 37.76 GHz, (c) 38.92 GHz.

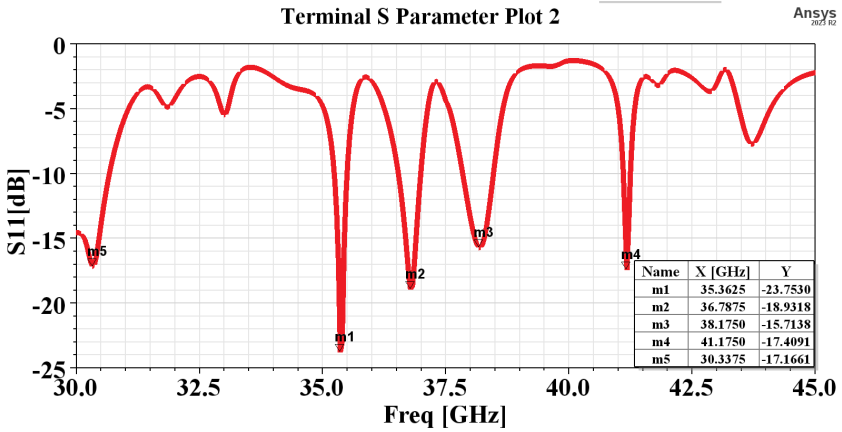

Figure 9. Reflection coefficient plot for the proposed antenna without PhC structure.

ranges, aiding in informed decision making during antenna design for various applications.

For comparison purposes, a new PhC configuration was designed by increasing the spacing between the photonic crystals and reducing the size of the square holes. Initially, the square hole side length was 0.2 mm. Then, it was reduced to 0.15 mm, while the spacing between the crystals was increased from 0.4 mm to 1.02 mm. In PhC structures, the periodicity and size of the structural features play a crucial role in determining how electromagnetic waves propagate and are guided. These changes resulted in an overall decrease in performance.

Gain measurements indicate that at 31.42 GHz, the gain is 4.02 dB, while at 37.76 GHz, the achieved gain is 4.32 dB, showing a noticeable reduction compared to the proposed design with square lattice. Although a slight improvement was observed at 38.92 GHz, the gain increased to 6.54 dB. The structural modifications caused an increase in energy loss through radiation, disrupted constructive interference, and led to greater reflection losses. As a result, less energy was effectively transmitted, leading to weak overall performance. The gain and reflection coefficient plots for this structure are shown in Fig. 12 and Fig. 13.

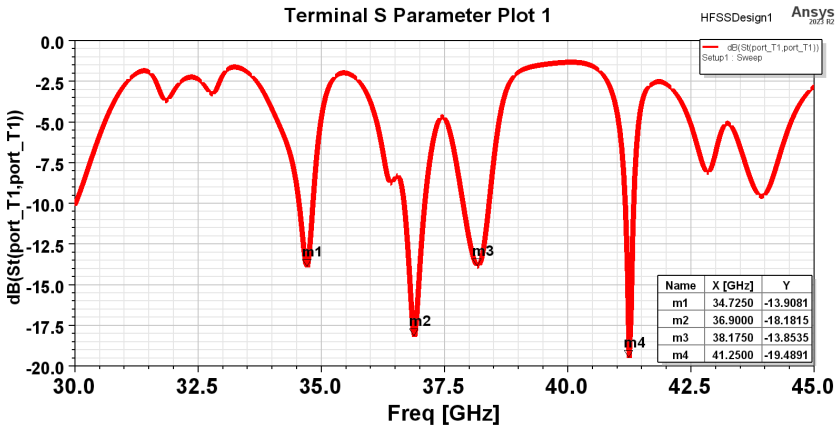

Figure 10. Reflection coefficient plot for the proposed PhC antenna with rectangular lattice structure

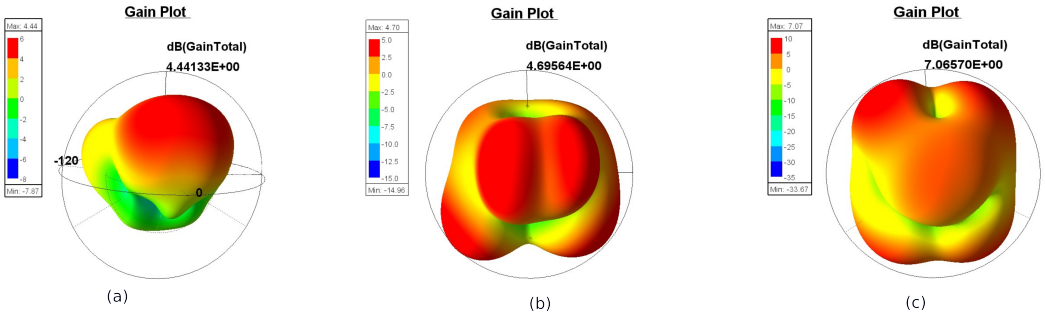

Figure 11. Gain plot of the proposed PhC antenna with rectangular lattice structure, at (a) 31.42 GHz, (b) 37.76 GHz, (c) 38.92 GHz.

3.1 Phantom Model Simulations for Vehicle Mounted Antenna Analysis

It is worthwhile to analyze the performance of the proposed antenna in realistic vehicular settings. Simulations were conducted to evaluate the performance of the proposed antenna mounted 2 mm on the rooftop of a vehicle. These simulations included a comparison of the antenna's mounted position on a car-like phantom model (whose length is 7 cm) and on a rooftop (size of 800 × 600 mm) without the car phantom model Fig. 15. Resulting 3D radiation patterns are also shown in these Figures. The simulation provides a realistic assessment of the antenna's ability to support both near-field and far-field coverage ranges. At 38.92 GHz, the gain decreases from 8.73 dB (for the proposed antenna alone) to 3.68 dB (small car) or 5.72 dB (car rooftop only). Values for the directivity are 4.00 dB and 5.81 dB for the small car and car rooftop only, respectively. Ensuring reliable signal propagation and stable field distribution in practical vehicular scenarios. These results demonstrate the antenna suitability for robust and consistent operation in real-world vehicular environments. As discussed in (Singh et al., 2017), (Imai et al., 2014), the level of detail in the phantom model significantly impacts the accuracy of the simulation results. Although a more detailed model could improve accuracy, it would also increase computational resource requirements and simulation time. These exploratory results aim to contribute and seek a balance

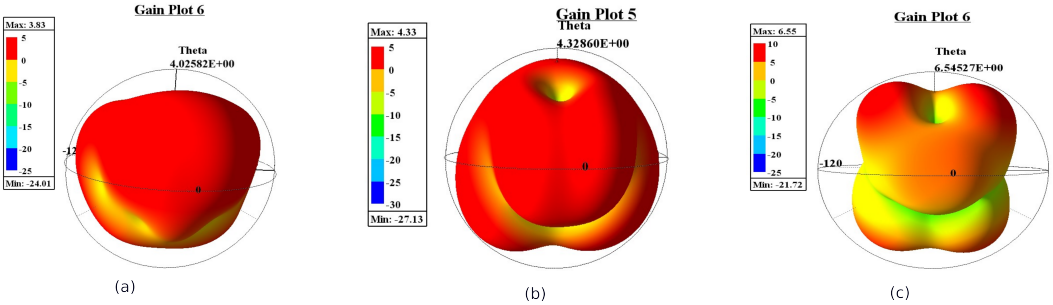

Figure 12. Gain plot of the PhC antenna with the hole side length reduced from 0.2 mm to 0.15 mm and the spacing between the crystals increased from 0.4 mm to 1.02 mm, at (a) 31.42 GHz, (b) 37.76 GHz, (c) 38.92 GHz.

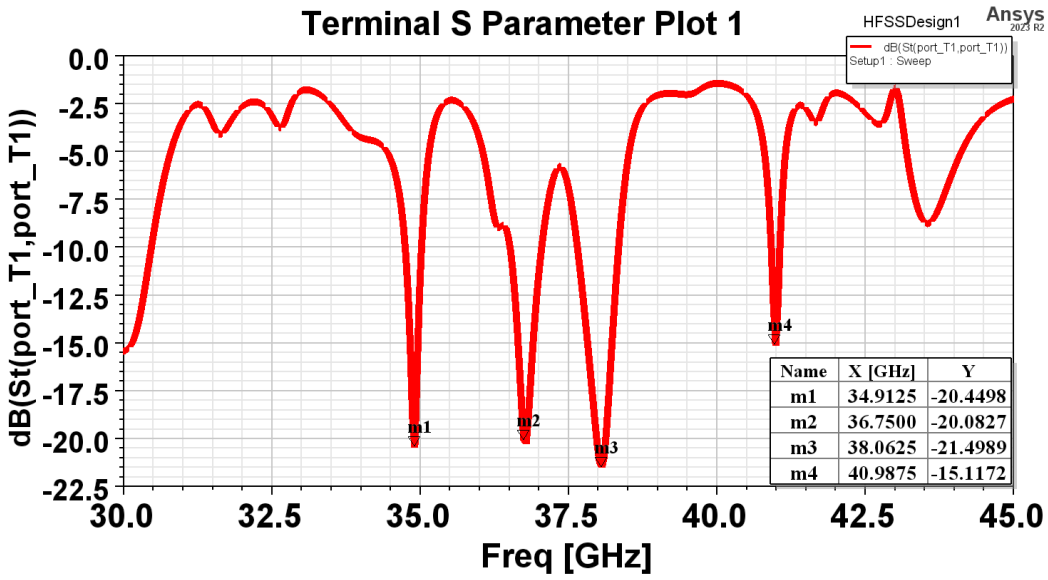

Figure 13. Reflection coefficient plot for the PhC antenna with the hole side length reduced from 0.2 mm to 0.15 mm and the spacing between the crystals increased from 0.4 mm to 1.02 mm.

between vehicle-mounted model complexity and its feasibility. Furthermore, validation will be achieved through fabrication and experimental measurements, which are left for future work.

4 Statement of Novelty

The paper presents an advancement in ITS through the development of a FPA integrated with PhC for V2X communication applications on the mmWaves. The antenna is designed to resonate at mmWaves as planed for V2X operations.

One of the key characteristics of this design lies in the seamless integration of PhC within the antenna structure. By intelligently incorporating PhC elements into the antenna substrate, the proposed design achieves enhanced radiation efficiency and improved communication performance in mmWaves

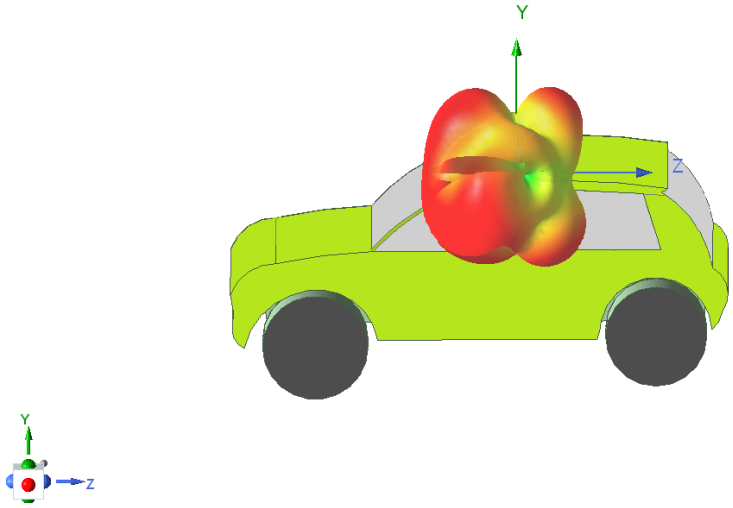

Figure 14. HFSS simulation of the PhC antenna on top of car phantom model, showing the antenna's 3D radiation pattern.

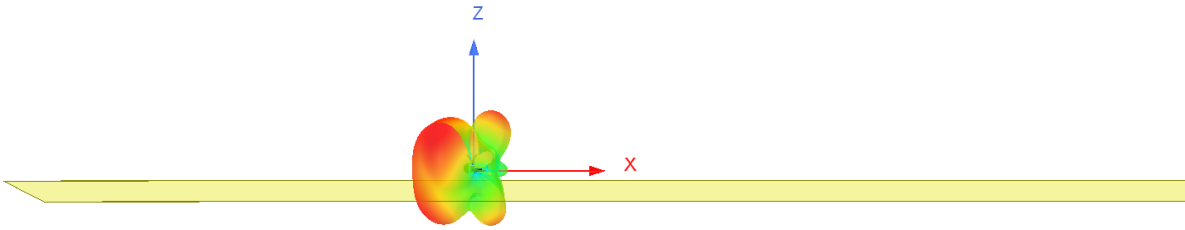

Figure 15. HFSS simulation of the PhC antenna of on top of the car rooftop, showing the antenna's 3D radiation pattern.

V2X scenarios. The PhC structure acts as a PBG, effectively prohibiting specific frequencies from propagating through the substrate, thereby improving antenna performance and mitigating undesired electromagnetic effects.

The bandwidth serves as a metric to determine the performance capacity of an antenna or communication system. A wider bandwidth typically results in higher data transmission rates, better signal quality, and enhanced communication capabilities.

Moreover, the utilization of GaAs as the substrate material is another pivotal aspect of the design. GaAs offers properties perfectly suited for millimeter-wave communication in V2X scenarios. Its wide bandwidth, low noise figure,

Table 1. Comparison of antenna performance from different studies/authors.

Material (ϵ_r)	f (GHz)	Gain(dBi)	Bandwidth (GHz)	Ref.
FR-4 (4.4)	1.50 2.45	2.14 -	9.70 -	(Kannappan et al., 2021)
TLY-5 (2.17-2.40)	28	7.41	1.5	(Park et al., 2016)
FR-4 (4.4)	26.5 28 35 39 43	4.93 - - - -	0.3 - - - -	(Mukherjee, Roy, & Mukhopadhyay, 2022)
GaAs (12.9)	31.42 37.76 38.92	6.54 10.63 10.88	1.73 0.38 0.78	(Bagheri, 2024)

Table 2. Performance Comparison of Different Antenna Configurations

Design Type	**Frequency (GHz)**	**Gain (dBd)**
Square Lattice	31.42	4.39
	37.76	8.48
	38.92	8.73
Without PhC	31.42	5.52
	37.76	4.58
	38.92	6.15
Rectangular Lattice	31.42	4.44
	37.76	4.69
	38.92	7.06
Square Lattice Modified Design	31.42	4.02
	37.76	4.32
	38.92	6.54

and high thermal conductivity contribute to the improved efficiency, reliability, and durability of the antenna system.

In addition, the integration of a PBG material within the GaAs substrate enables precise control over electromagnetic wave propagation, resulting in improved radiation efficiency, thus enhancing overall communication performance in ITS applications. The synergistic integration of PhC structures and GaAs substrate material represents a significant leap forward in the field of ITS communication antenna design. The approach promises to revolutionize the ITS landscape, facilitating the foundation for more robust and efficient ITS communication networks.

5 Conclusion

Lately, there has been a notable trend in commercial and communication systems toward the development of low-cost, lightweight, and low-profile

antennas capable of maintaining excellent performance across a wide frequency range. This technological shift has brought significant attention to antenna design, with a particular focus on novel configurations such as fractal nonagonal antennas.

Nonagonal fractal antennas offer several benefits over traditional designs. These include low cost, compact size, ease of fabrication and installation, and compatibility with integrated circuit technology. The nonagonal fractal antenna proposed in this paper utilizes several advantages, including compact size, affordability, and high efficiency. With a bandwidth of 2.89 GHz and a gain of 10.88 dBi at the 38.92 GHz resonance frequency, this antenna is particularly suitable for V2X applications within the FR2 frequency range. Its properties position it as a potential candidate for various communication applications, including K_a-band and FR2 communications, V2X communications, and satellite communications.

Future research will involve the fabrication and testing of the designed antenna in real-world environments, after the antenna fabrication, we plan to conduct detailed measurements of the S11 response, radiation pattern, and VSWR by using an EMI/EMC testing facility.

Exploring the use of Barium Strontium Titanate (BST) material for the antenna substrate offers additional benefits, such as high dielectric constant and tunable permittivity, enabling miniaturization and improved performance in vehicular environments. Combining BST with photonic crystal structures enhances radiation efficiency and reduces interference while maintaining high performance for millimeter-wave V2X applications. Leveraging BST and photonic crystals can achieve superior impedance matching and enhanced communication capabilities, contributing to the evolution of ITS. Additionally, BST's tunable properties enable dynamic adaptation to changing environmental conditions, further enhancing the antenna's versatility and effectiveness in V2X.

Acknowledgment

This work is co-financed by Fundação para a Ciência e a Tecnologia, I.P. (Portuguese Foundation for Science and Technology) through the Carnegie Mellon Portugal Program under the fellowship PRT/BD/154686/2023 and FCT/MECI through national funds and when applicable co-funded EU funds under UID/50008: Instituto de Telecomunicações, COST CA20120 INTERACT, BID UBI-Santander Totta fellowship 2022/2023 and TeamUp5G. TeamUp5G project has received funding from the European Union's Horizon 2020 research.

Data Availability Statement

This study does not involve the use of new data.

References

3GPP. (2021, March). *TR 38.808: Study on supporting NR from 52.6 GHz to 71 GHz* (Tech. Spec. No. 17.0.0). 3rd Generation Partnership Project (3GPP).

3rd Generation Partnership Project (3GPP). (2023, June). *TS 38.101-2: NR; User Equipment (UE) radio transmission and reception; Part 2: Range 2 Standalone* (Tech. Spec.) Author. (Release 18, version 18.2.0)

Ahangar, M. N., Ahmed, Q. Z., Khan, F. A., & Hafeez, M. (2021). A Survey of Autonomous Vehicles: Enabling Communication Technologies and Challenges. *Sensors*, *21*(3). Retrieved from https://www.mdpi.com/1424-8220/21/3/706 doi: 10.3390/s21030706.

Ahmad, I., Farooque, U., & Hameed, A. (2020). Pin Loaded Triangular Patch Antenna with Embedded Spurline for Enhanced Antenna Gain. In *2020 International Youth Conference on Radio Electronics, Electrical and Power Engineering (REEPE)* (p. 1-5). doi: 10.1109/REEPE49198.2020.9059169.

Ansys. (2023). *High-Frequency Structural Simulator (HFSS).* Retrieved 2 May 2024, from https://www.ansys.com/products/electronics/ansys-hfss

Asok, A. O., & Dey, S. (2021). UWB Antipodal Antenna With Parasitic Patch and Elliptical Cylindrical Dielectric For Concealed Object Detection with Microwave Imaging. In *2021 IEEE International Symposium on Antennas and Propagation and USNC-URSI Radio Science Meeting (APS/URSI)* (p. 741-742). doi: 10.1109/APS/URSI47566.2021.9704371.

Awan, W. A., Alibakhshikenari, M., & Limiti, E. (2021). High Gain Dual Parasitic Patch Loaded Wideband Antenna for 28 GHz 5G Applications. In *2021 International Symposium on Antennas and Propagation (ISAP)* (p. 1-2). doi: 10.23919/ISAP47258.2021.9614441.

Bagheri, N. (2024). Fractal Patch Antenna based on Photonic Crystal for Enhanced Millimeter-Wave Communication in Intelligent Transportation Systems. *Journal Name*.

Bagheri, N., Teixeira, E., Velez, F. J., & Peha, J. M. (2024). Multi-Band Resonant Photonic Crystal Antenna for 5G Applications. In *2024 IEEE 22nd Mediterranean Electrotechnical Conference (MELECON)* (p. 526-531). doi: 10.1109/MELECON56669.2024.10608697.

Bakir, S. S., & Sahin, A. B. (2023). Non-Destructive Defect Detection on PCB Boards Using a Metamaterial-Based Circular Patch Antenna. In *2023 Innovations in Intelligent Systems and Applications Conference (ASYU)* (p. 1-4). doi: 10.1109/ASYU58738.2023.10296552.

Benlakehal, M. E., Hocini, A., Khedrouche, D., Temmar, M. N., Denidni, T. A., & Shayea, I. (2023, Jun 01). Design and analysis of a 1 × 2 microstrip patch antenna array based on photonic crystals with a graphene load in THZ. *Journal of Optics*, *52*(2), 483-493. doi: 10.1007/s12596-022-01006-8.

Benlakehal, M. E., Hocini, A., Khedrouche, D., Temmar, M. N. e., & Denidni, T. A. (2022, Sep 13). Design and analysis of MIMO system for THz communication using terahertz patch antenna array based on photonic crystals with graphene. *Optical and Quantum Electronics*, *54*(11), 693. doi: 10.1007/s11082-022-04081-0.

Benlakehal, M. E., Hocini, A., Khedrouche, D., Temmar, M. N. e., Denidni, T. A., & Shayea, I. (2024, Feb 01). Design and simulation of 1 × 2, 1 × 4 and 2 × 8 microstrip patch antenna arrays based on photonic crystals for improved gain performance in THz. *Journal of Optics*, *53*(1), 260-271. Retrieved from https://doi.org/10.1007/s12596-023-01513-2. doi: 10.1007/s12596-023-01513-2.

Biswas, M., Ghosh, S., Mitra, C., & Gupta, B. (2023). Design and Performance Analysis of Defected Grounded Hexagonal Patch Antenna at 5.17 GHz. In *2023 International Conference on Computer, Electronics & Electrical Engineering & their Applications (IC2E3)* (p. 1-4). doi: 10.1109/IC2E357697.2023.10262464.

Chen, C. (2022). A Wideband Coplanar L-Probe-Fed Slot-Loaded Rectangular Filtering Microstrip Patch Antenna With High Selectivity. *IEEE Antennas and Wireless Propagation Letters*, *21*(6), 1134-1138. doi: 10.1109/LAWP.2022.3159230.

Chen, S., He, X., Zhao, R., Hu, J., & Zhang, X. (2024). Building mmWave on the evolving C-V2X: MmWave NR-V2X. *China Communications*, *21*(1), 88-101. doi: 10.23919/JCC.fa.2023-0351.202401.

Desai, P. K., & Bindu, S. (2023). Impact of Dielectric Substrate on the performance of Microstrip Patch Antenna at millimeter wave frequency. In *2023 International Conference on Intelligent and Innovative Technologies in Computing, Electrical and Electronics (IITCEE)* (p. 629-632). doi: 10.1109/IITCEE57236.2023.10091083.

Deshmukh, R., Marathe, D., & Kulat, K. D. (2019). Microstrip Patch Antenna Gain Enhancement using Near-zero Index Metamaterial Superstrate (NZIM Lens). In *2019 10th International Conference on Computing, Communication and Networking Technologies (ICCCNT)* (p. 1-6). doi: 10.1109/ICCCNT45670.2019.8944470.

Dong, N., Qi, N., Guo, M., Wang, C., & Chen, L. (2022). An Optimal Design of High Gain Beidou Anti-Jamming Antenna. In *2022 International Symposium on Networks, Computers and Communications (ISNCC)* (p. 1-4). doi: 10.1109/ISNCC55209.2022.9851746.

El Arrouch, T., El Amrani El Idrissi, N., & El Ansari, A. (2022). Microstrip Patch Antenna using a Parasitic Mushroom for 5GApplication at 28GHz. In *2022 9th International Conference on Wireless Networks and Mobile Communications (WINCOM)* (p. 1-6). doi: 10.1109/WINCOM55661.2022.9966479.

Erbaş, C. D. (2020). Parametric Analysis of Angular Rotation for Microstrip Patch Antenna with Elliptical Patch and Parasitic Elements. In *2020 International Conference on Electrical, Communication, and Computer Engineering (ICECCE)* (p. 1-6). doi: 10.1109/ICECCE49384.2020.9179237.

Fang, Y., Wu, L.-S., Qiu, L.-F., & Zhang, Y. P. (2022). A Method of Introducing Coupling Null by Shorting Pins for Stacked Microstrip Patch Antenna Array. *IEEE Transactions on Antennas and Propagation*, *70*(7), 6030-6035. doi: 10.1109/TAP.2022.3161315.

Garcia, M. H. C., Molina-Galan, A., Boban, M., Gozalvez, J., Coll-Perales, B., Şahin, T., & Kousaridas, A. (2021). A Tutorial on 5G NR V2X Communications. *IEEE Communications Surveys & Tutorials*, *23*(3), 1972-2026. doi: 10.1109/COMST.2021.3057017.

Gautam, S. K., & Kumar, A. (2023). High Gain Dual-Band Shorting Pins Loaded Microstrip Patch Antenna. In *2023 IEEE Wireless Antenna and Microwave Symposium (WAMS)* (p. 1-4). doi: 10.1109/WAMS57261.2023.10242876.

Gyawali, S., Xu, S., Qian, Y., & Hu, R. Q. (2021). Challenges and Solutions for Cellular Based V2X Communications. *IEEE Communications Surveys & Tutorials*, *23*(1), 222-255. doi: 10.1109/COMST.2020.3029723.

Hakak, S., Gadekallu, T. R., Maddikunta, P. K. R., Ramu, S. P., M, P., De Alwis, C., & Liyanage, M. (2023). Autonomous vehicles in 5G and beyond: A survey. *Vehicular Communications*, *39*, 100551. Retrieved from `https://www.sciencedirect.com/science/article/pii/S2214209622000985` doi: https://doi.org/10.1016/j.vehcom.2022.100551.

Hamza, A., Chaabane, A., & Attia, H. (2022). Gain Improvement of Wideband Patch Antenna at Millimeter-wave Band Using Novel Metamaterial Superstrate. In *2022 16th European Conference on Antennas and Propagation (EuCAP)* (p. 1-4). doi: 10.23919/EuCAP53622.2022.9769308.

Hao, S.-S., Chen, Q.-Q., Li, J.-Y., & Xie, J. (2020). A High-Gain Circularly Polarized Slotted Patch Antenna. *IEEE Antennas and Wireless Propagation Letters*, *19*(6), 1022-1026. doi: 10.1109/LAWP.2020.2987330.

Hossain, A. R., Nguyen, T., & Karacolak, T. (2021). A Parasitic Patch Antenna System with High Isolation for Full Duplex Application. In *2021 IEEE Texas Symposium on Wireless and Microwave Circuits and Systems (WMCS)* (p. 1-3). doi: 10.1109/WMCS52222.2021.9493280.

Howell, J. (1975). Microstrip antennas. *IEEE Transactions on Antennas and Propagation*, *23*(1), 90-93. doi: 10.1109/TAP.1975.1141009.

Imai, S., Taguchi, K., Kashiwa, T., & Kawamura, T. (2014). Effects of car body on radiation pattern of car antenna mounted on side mirror for inter-vehicle communications. In *2014 IEEE Antennas and Propagation Society International Symposium (APSURSI)* (p. 601-602). doi: 10.1109/APS.2014.6904631.

Jiang, H., Yan, N., Ma, K., & Wang, Y. (2023). A Wideband Circularly Polarized Dielectric Patch Antenna With a Modified Air Cavity for Wi-Fi 6 and Wi-Fi 6E Applications. *IEEE Antennas and Wireless Propagation Letters*, *22*(1), 213-217. doi: 10.1109/LAWP.2022.3201077.

K, A. S. B., & Pradeep, A. (2022). Complementary Metamaterial Superstrate for Wide Band High Gain Antenna. In *2022 IEEE Wireless Antenna and Microwave Symposium (WAMS)* (p. 1-5). doi: 10.1109/WAMS54719.2022.9847735.

Kannappan, L., Palaniswamy, S. K., Wang, L., Kanagasabai, M., Kumar, S., Alsath, M. G. N., & Rao, T. R. (2021). Quad-Port Multiservice Diversity Antenna for Automotive Applications. *Sensors*, *21*(24). Retrieved from `https://www.mdpi.com/1424-8220/21/24/8238` doi: 10.3390/s21248238.

Khabba, A., Wakrim, L., El Ouadi, Z., Amadid, J., Ibnyaich, S., & Zeroual, A. (2022). High Gain Double U-shaped Slots Microstrip Patch Antenna Array For 28GHz 5G Applications. In *2022 International Conference on Decision Aid Sciences and Applications (DASA)* (p. 1589-1592). doi: 10.1109/DASA54658.2022.9765096.

Kulkarni, P. P., & Deshpande, V. S. (2024). High Gain Metamaterial Superstrate Loaded Antenna For S band Communication. In *2024 IEEE Radio and Wireless Symposium (RWS)* (p. 140-142). doi: 10.1109/RWS56914.2024.10438511.

Kumar, D. S., Pavithra, S., Ranjith, K., Kiruthika, R., & Kavin, E. (2023). Design and Investigation of Metamaterial Antenna for Wireless Communication. In *2023 7th International Conference on Electronics, Communication and Aerospace Technology (ICECA)* (p. 1464-1468). doi: 10.1109/ICECA58529.2023.10395476.

Li, W., Ren, J., Zhang, B., Liu, Y.-T., Zhang, H., Yin, Y., & Shen, M. (2023). Wideband Dielectric Patch Antenna With Stable Radiation Pattern. *IEEE Antennas and Wireless Propagation Letters*, *22*(7), 1716-1720. doi: 10.1109/LAWP.2023.3261506.

Ligo, A. K., & Peha, J. M. (2019). Spectrum for V2X: Allocation and Sharing. *IEEE Transactions on Cognitive Communications and*

Networking, *5*(3), 768-779. doi: 10.1109/TCCN.2019.2916026.

Lin, H.-Y., & Omote, H. (2021). An analysis of increasing the gain of the patch antenna using slots on the ground plane. In *2020 International Symposium on Antennas and Propagation (ISAP)* (p. 561-562). doi: 10.23919/ISAP47053.2021.9391348.

Mangal, J., & Gour, Y. (2021). A High Gain Planar Monopole Hexagonal Circular Slotted Patch Antenna For Ultra-Wideband And Multiple Frequency Range Applications. In *2021 International Conference on Control, Automation, Power and Signal Processing (CAPS)* (p. 1-4). doi: 10.1109/CAPS52117.2021.9730637.

Messatfa, T., Chebbara, F., & Annou, A. (2022). Analysis and Design of Printed Antenna Based on Photonic Crystal Substrate for 5 GHz Applications. In *2022 19th International Multi-Conference on Systems, Signals & Devices (SSD)* (p. 2070-2073). doi: 10.1109/SSD54932.2022.9955813.

Mishra, P., Komatineni, R., & Kulat, K. D. (2023). Millimeter Wave MPA using Metamaterial-Substrate Antenna Array for Gain Enhancement. In *2023 National Conference on Communications (NCC)* (p. 1-4). doi: 10.1109/NCC56989.2023.10068072.

Muangrung, B., Lang, A., Torrungrueng, D., Phongcharoenpanich, C., & Kawdungta, S. (2023). Compact High-Gain Dual-band Patch Antenna With Dielectric Superstrate for Wi-Fi 6 Applications. In *2023 International Electrical Engineering Congress (iEECON)* (p. 76-79). doi: 10.1109/iEECON56657.2023.10126809.

Mukherjee, K., Das, A., & Roy, S. (2020). Comparative study on a u-slot miniaturized cpw-fed multi-band antenna applicable for 5g communication. In P. K. Mallick, P. Meher, A. Majumder, & S. K. Das (Eds.), *Electronic systems and intelligent computing* (pp. 707–718). Singapore: Springer Singapore.

Mukherjee, K., Mukhopadhyay, S., & Roy, S. (2022). Design of wideband planar antenna with inverted I-shaped tuning stubs for application in 5G, satellite communication, and Internet of Things. *International Journal of Communication Systems*, *35*. Retrieved from `https://api.semanticscholar.org/CorpusID:249680095`.

Mukherjee, K., Roy, S., & Mukhopadhyay, S. (2022). A SISO Y-Shape 5G Antenna for Intelligent Transportation Systems. In *2022 Second International Conference on Computer Science, Engineering and Applications (ICCSEA)* (p. 1-6). doi: 10.1109/ICCSEA54677.2022.9936517.

Niranjan Prasad, J. N., Nirmal Kumar, R. G., Nirmal Kishore, A., & Jayaram, M. (2023). Tesla-geometry based wideband 5G antenna for V2V applications. In *2023 International Conference on Networking and Communications (ICNWC)* (p. 1-4). doi: 10.1109/ICNWC57852.2023.10127489.

Olawoye, T. O., & Kumar, P. (2020). A High Gain Microstrip Patch Antenna with Slotted Ground Plane for Sub-6 GHz 5G Communications. In *2020 International Conference on Artificial Intelligence, Big Data, Computing and Data Communication Systems (icABCD)* (p. 1-6). doi: 10.1109/icABCD49160.2020.9183820.

Oliveira, T. E. S., Goncalves, J. F., Reis, J. R., Vala, M., & Caldeirinha, R. F. S. (2021). High-Gain Wideband Parasitic Microstrip Antenna for 5G and IoT at 26 GHz. In *2021 Telecoms Conference (ConfTELE)* (p. 1-5). doi: 10.1109/ConfTELE50222.2021.9435457.

Park, J.-S., Ko, J.-B., Kwon, H.-K., Kang, B.-S., Park, B., & Kim, D. (2016). A Tilted Combined Beam Antenna for 5G Communications

Using a 28-GHz Band. *IEEE Antennas and Wireless Propagation Letters*, *15*, 1685-1688. doi: 10.1109/LAWP.2016.2523514.

Peha, J. M. (2023). Bringing Connected Vehicle Communications (V2X) to Shared Spectrum. In *2023 19th international conference on wireless and mobile computing, networking and communications (wimob)* (p. 431-437). doi: 10.1109/WiMob58348.2023.10187776.

Peha, J. M., Jin, Z., & de Koo, W. (2024). Vehicle-to-Everything (V2X) Communications in Unlicensed Spectrum Can Be Safe and Efficient. *IEEE Access*, *12*, 181179-181191. doi: 10.1109/ACCESS.2024.3508595.

Roslan, N. H., Awang, A. H., & Hizan, H. M. (2018). The Effect of Photonic Crystal Parameters on The Terahertz Photonic Crystal Cavities Microstrip Antenna Performances. In *2018 IEEE International RF and Microwave Conference (RFM)* (p. 147-150). doi: 10.1109/RFM.2018.8846486.

Saad, M. M., Khan, M. T. R., Shah, S. H. A., & Kim, D. (2021). Advancements in Vehicular Communication Technologies: C-V2X and NR-V2X Comparison. *IEEE Communications Magazine*, *59*(8), 107-113. doi: 10.1109/MCOM.101.2100119.

Saad, M. M., Tariq, M. A., Seo, J., & Kim, D. (2023). An overview of 3gpp release 17 & 18 advancements in the context of v2x technology. In *2023 International Conference on Artificial Intelligence in Information and Communication (ICAIIC)* (p. 057-062). doi: 10.1109/ICAIIC57133.2023.10067121.

Salehi, M., Abbasian, K., & Pourziad, A. (2020). 2D-Photonic Crystal Based Bowtie Nano Antenna Designing with Spherical Gold Particles for Terahertz Applications. In *2020 28th Iranian Conference on Electrical Engineering (ICEE)* (p. 1-4). doi: 10.1109/ICEE50131.2020.9261027.

Saurabh, A. K., & Meshram, M. K. (2022). Integration of Sub-6 GHz and mm-Wave Antenna for Higher-Order 5G-MIMO System. *IEEE Transactions on Circuits and Systems II: Express Briefs*, *69*(12), 4834-4838. doi: 10.1109/TCSII.2022.3197598.

Sharma, R., Raghava, N., & De, A. (2021). Design of Compact Circular Microstrip Patch Antenna using Parasitic Patch. In *2021 6th International Conference for Convergence in Technology (I2CT)* (p. 1-4). doi: 10.1109/I2CT51068.2021.9418104.

Singh, J., Asgharzadeh, A., Stephan, R., & Hein, M. A. (2017). Influence of Car Body Modeling on the Gain Patterns of Automotive Antennas. In *2017 IEEE 85th Vehicular Technology Conference (VTC Spring)* (p. 1-5). doi: 10.1109/VTCSpring.2017.8108214.

Sinha, P. D., Ghosh, B., & Deepa, B. (2021). Gain Enhancement of Patch Antenna Array Using a Metamaterial Superstrate. In *2021 IEEE International Symposium on Antennas and Propagation and USNC-URSI Radio Science Meeting (APS/URSI)* (p. 251-252). doi: 10.1109/APS/URSI47566.2021.9704344.

Soily, S., Alam, M. J., & Latif, S. I. (2022). A High Gain Circularly Polarized Pin Loaded Microstrip Patch Antenna with DNG Metamaterial as Superstrate. In *2022 IEEE International Symposium on Antennas and Propagation and USNC-URSI Radio Science Meeting (AP-S/URSI)* (p. 1454-1455). doi: 10.1109/AP-S/USNC-URSI47032.2022.9887268.

Soto, I., Calderon, M., Amador, O., & Urueña, M. (2022). A survey on road safety and traffic efficiency vehicular applications based on C-V2X technologies. *Vehicular Communications*, *33*, 100428.

Retrieved from https://www.sciencedirect.com/science/article/pii/S2214209621000978 doi: https://doi.org/10.1016/j.vehcom.2021.100428.

Sufian, M. A., Hussain, N., Askari, H., Park, S. G., Shin, K. S., & Kim, N. (2021). Isolation Enhancement of a Metasurface-Based MIMO Antenna Using Slots and Shorting Pins. *IEEE Access*, *9*, 73533-73543. doi: 10.1109/ACCESS.2021.3079965.

Tanveer, S., Rashid, A., & Ur-Rehman, M. (2021). A Millimeter-wave Broadband Magneto-electric Dipole Antenna Using Complementary Back Reflectors and Air-gaps. In *2021 1st International Conference on Microwave, Antennas & Circuits (ICMAC)* (p. 1-4). doi: 10.1109/ICMAC54080.2021.9678296.

Temmar, M. N., Nedil, M., & Chehri, A. (2023). Analysis and Design of Terahertz Elliptical Slot Antenna Based on Photonic Crystal Substrate. In *2023 IEEE International Symposium on Antennas and Propagation and USNC-URSI Radio Science Meeting (USNC-URSI)* (p. 197-198). doi: 10.1109/USNC-URSI52151.2023.10237916.

U.S. Department of Transportation (October). (2024, October). *ITS JPO Blog: Demonstrating Interoperability for Safer Transportation.* Retrieved from https://www.its.dot.gov/communications/blogs/itsjpo_directors_blog_17.htm (Accessed 2024, October)

Vahdati, A., & Parandin, F. (2019, Dec 01). Antenna Patch Design Using a Photonic Crystal Substrate at a Frequency of 1.6THz. *Wireless Personal Communications*, *109*(4), 2213-2219. Retrieved from https://doi.org/10.1007/s11277-019-06676-5 doi: 10.1007/s11277-019-06676-5.

Wu, D.-L., Chen, J. H., Yang, K. Y., Zhu, W. J., & Ye, L. H. (2023). A Compact Dual-Polarized Patch Antenna With L-Shaped Short Pins. *IEEE Antennas and Wireless Propagation Letters*, *22*(4), 689-693. doi: 10.1109/LAWP.2022.3222338.

Yan, T.-Y., Ding, X.-H., Yang, J.-Y., & Chen, J.-X. (2024). A Low-Cost Compact Dual-Polarized Patch Antenna Array for 5G Massive MIMO Base Station. *IEEE Antennas and Wireless Propagation Letters*, *23*(4), 1381-1385. doi: 10.1109/LAWP.2024.3356531.

Yang, Y., Zhang, X., Tan, T., Zhu, L., & Yuan, T. (2021). A Pin-Loaded and SIW-Fed Circular Patch Antenna with Stable High Gain and Wide Impedance Bandwidth. In *2021 Cross Strait Radio Science and Wireless Technology Conference (CSRSWTC)* (p. 304-306). doi: 10.1109/CSRSWTC52801.2021.9631748.

Ye, J., Jiang, Y., & Ge, X. (2024). Deep Reinforcement Learning Assisted Hybrid Precoding for V2I Communications with Doppler Shift and Delay Spread. *IEEE Transactions on Vehicular Technology*, 1-16. doi: 10.1109/TVT.2024.3370602.

Yin, J., Chen, Z. N., Wang, H., Lou, Q., & Lai, B. (2023). Single-Mode Dual-Band Patch Antenna Based on the Lorentz Model of Dispersive Metamaterials. *IEEE Transactions on Antennas and Propagation*, *71*(11), 8580-8591. doi: 10.1109/TAP.2023.3314214.

Zhang, D., Wang, Y., Li, X., & Xiang, W. (2018). Hybridly Connected Structure for Hybrid Beamforming in mmWave Massive MIMO Systems. *IEEE Transactions on Communications*, *66*(2), 662-674. doi: 10.1109/TCOMM.2017.2756882.

Zhang, J., & Mao, J. (2020). A High-Gain Ka-Band Microstrip Patch Antenna with Simple Slot Structure. In *2020 International Conference on Microwave and Millimeter Wave Technology (ICMMT)* (p. 1-3). doi: 10.1109/ICMMT49418.2020.9386991.

Zhang, X., Tan, T.-Y., Wu, Q.-S., Zhu, L., Zhong, S., & Yuan, T. (2021). Pin-Loaded Patch Antenna Fed With a Dual-Mode SIW Resonator for Bandwidth Enhancement and Stable High Gain. *IEEE Antennas and Wireless Propagation Letters*, *20*(2), 279-283. doi: 10.1109/LAWP.2020.3048749.

Zhao, Z., Wu, L.-S., & Mao, J.-F. (2023). Ka-Band Stacked Patch Antenna Array on Multilayer Silicon Interposer for Three-Dimensional Integration. In *2023 International Conference on Microwave and Millimeter Wave Technology (ICMMT)* (p. 1-3). doi: 10.1109/ICMMT58241.2023.10277596.